JOURNAL OF THERMOPHYSICS AND HEAT TRANSFER
Vol. 11, No. 4, October–December 1997

Technical Notes

TECHNICAL NOTES are short manuscripts describing new developments or important results of a preliminary nature. These Notes cannot exceed 6 manuscript pages and 3 figures; a page of text may be substituted for a figure and vice versa. After informal review by the editors, they may be published within a few months of the date of receipt. Style requirements are the same as for regular contributions (see inside back cover).

Visualization Study of Flooding and Entrainment in a Closed Two-Phase Thermosyphon

D. P. Shatto,* J. A. Besly,* and G. P. Peterson†
Texas A&M University, College Station, Texas 77843

Nomenclature

Bo = Bond number
C_{fi} = friction coefficient
C_K = defined by Eq. (7)
c_w = empirical constant
D = internal diameter, m
g = gravitational acceleration, m/s^2
h_{fg} = heat of vaporization, J/kg
j = superficial velocity, m/s
K = Kutateladze parameter
L = length, m
$\dot{m}$ = mass flow rate, kg/s
Q = heat transport rate, W
R = inner radius, m
δ = film thickness, m
μ = viscosity, N s/m^2
ρ = density, kg/m^3
σ = surface tension, N/m
τ_i = interfacial shear, N/m^2

Subscripts
e = evaporator
L = liquid
v = vapor

Introduction

THE requirement of only small temperature gradients to accommodate large heat transport rates makes thermosyphons efficient devices for thermal control. Fast thermal response and the utilization of phase changes in the working fluid allow thermosyphons to operate at nearly isothermal conditions for a wide range of power inputs, thereby motivating their use in a wide range of applications, including the protection of permafrost under the Alaska oil pipeline, microelectronics cooling, and heat exchangers for industrial regeneration processes.[1]

The maximum heat transport capacity of a thermosyphon can be limited by a number of phenomena, including 1) sonic flow (choking) of the vapor as it enters the condenser, 2) film boiling of the liquid in the evaporator, 3) flooding of the condenser caused by shear stress at the liquid–vapor interface, and 4) entrainment of droplets from the liquid flow into the vapor stream. Flooding and entrainment are the most commonly encountered limitations, and usually act together to inhibit liquid flow in the thermosyphon.

Previous investigators have pursued several means to predict the onset of flooding and entrainment with varying success, but few studies have combined accurate heat transfer measurements with visualization of the physical phenomena involved. The predictions of existing correlations vary considerably. Visualization improves the accuracy of data collection since the onset of flooding and entrainment receive different interpretations through measurement alone. The assumption has often been made that flooding causes dryout in portions of the evaporator and a subsequent decrease in the heat transport rate. In previous investigations, changes in thermocouple readings of vapor and liquid temperatures indicated the onset of entrainment and instability of the liquid film on the thermosyphon wall. Oscillation of these temperatures has been cited as a clear indication of dryout. Although it is true that dryout has an adverse effect on heat transfer, evidence suggests that flooding and/or entrainment may occur well before dryout. The current study focuses on the onset of flooding and entrainment limitations of thermosyphons caused by viscous shear forces at the liquid–vapor interface.

Theory

The correlations considered in the present study can be classified according to the theoretical basis on which the correlation is constructed.

Predictions Based on Flooding Correlations

Tien and Chung[2] developed a flooding limit prediction based on two previous countercurrent flooding correlations. The first of these is the Wallis correlation:

$$\sqrt{j_v^*} + \sqrt{j_L^*} = c_w \tag{1}$$

where $c_w \approx 0.7$–1.0, and the dimensionless superficial velocities are defined as follows:

$$j_i^* \equiv \sqrt{\frac{\rho_i j_i^2}{gL(\rho_L - \rho_v)}} \tag{2}$$

where the characteristic dimension L was typically set equal to the i.d. of the tube. The superficial velocities of the two phases can be related through the overall mass and energy balance:

$$\frac{4Q}{\pi D^2 h_{fg}} = \rho_L \cdot j_L = \rho_v \cdot j_v \tag{3}$$

The other flooding correlation considered by Tien and Chung[2] can be expressed in terms of the dimensionless groups proposed by Kutateladze and Sorokin[3]:

$$\sqrt{K_v} + \sqrt{K_L} = \sqrt{3.2} \tag{4}$$

Presented as Paper 96-1832 at the AIAA 31st Thermophysics Conference, New Orleans, LA, June 17–20, 1996; received July 1, 1996; revision received April 1, 1997; accepted for publication April 13, 1997.

*Graduate Research Assistant, Department of Mechanical Engineering.
†Associate Vice-Chancellor of Engineering. Associate Fellow AIAA.

where

$$K_i \equiv \sqrt{\rho_i} j_i / [g\sigma(\rho_L - \rho_v)]^{1/4} \quad (5)$$

Tien and Chung[2] noted that these two flooding correlations are equivalent if the characteristic dimension L is set equal to the critical wavelength of Taylor instability. Equation (4) predicts that the superficial velocities corresponding to the flooding condition are independent of the diameter of the flow channel. This is known to be inaccurate for small-diameter tubes, where Eq. (1), with $L = D$, yields more accurate predictions. The applicability of these two predictions depends on the Bond number, a dimensionless tube diameter, defined as

$$Bo \equiv D\sqrt{g(\rho_L - \rho_v)/\sigma} \quad (6)$$

To correct for the reduction in the flooding limit at small values of the Bond number, Tien and Chung[2] proposed replacing the constant in Eq. (4) with a function that decreases with decreasing Bo:

$$\sqrt{K_v} + \sqrt{K_L} = C_K = \sqrt{3.2}\tanh(Bo^{1/4}/2) \quad (7)$$

Combining Eq. (7) with the overall mass and energy balance, Eq. (3) yields a prediction for the heat transport limit caused by flooding in a closed two-phase thermosyphon:

$$Q = \frac{(\pi C_K^2 D^2 h_{fg}/4)[g\sigma(\rho_L - \rho_v)]^{1/4}}{(1/\rho_L^{1/4} + 1/\rho_v^{1/4})^2} \quad (8)$$

Shiriashi et al.[4] evaluated a similar correlation obtained by Nejat,[5] in which the Bond number dependence has been simplified and a term included to account for the effects of the evaporator length-to-diameter ratio:

$$\frac{Q}{\pi D L_e \rho_v h_{fg}} = \frac{0.09[\sigma g(\rho_L - \rho_v)/\rho_v^2]^{1/4}(D/L_e)^{0.9}\sqrt{Bo}}{[1 + (\rho_v/\rho_L)^{1/4}]^2} \quad (9)$$

Faghri et al.[6] noted that the Tien and Chung correlation[2] tends to underpredict the flooding limit when the liquid/vapor density ratio is high. This discrepancy was especially evident in experiments with water. It was proposed that the constant C_K in the Kutateladze flooding correlation, which was expressed as a function of the Bond number by Tien and Chung,[2] should also exhibit the following dependence on the liquid and vapor densities:

$$C_K^2 = (\rho_L/\rho_v)^{0.14}\tanh^2(Bo^{1/4}) \quad (10)$$

Correlation Based on Dimensional Analysis

Imura et al.[7] examined previous efforts to develop correlations of critical heat flux in confined channels based on dimensional analysis, and proposed the following equation that correlated most available data to within ±30%:

$$Q = 0.64(\pi D^2/4)(\rho_L/\rho_v)^{0.13} h_{fg}[\sigma g \rho_v^2(\rho_L - \rho_v)]^{1/4} \quad (11)$$

Prediction Based on Interfacial Shear Balance

Some researchers[8,9] have presented analytical models in which the downward flow of the liquid film is balanced by friction forces at the liquid–vapor interface and at the tube wall. Katto and Watanabe[8] assumed that the liquid film thickness can be neglected when calculating the mean vapor velocity, and that the vapor/liquid density ratio is very small. Performing the same analysis as that of Nusselt for laminar liquid film flow on a vertical flat wall, they obtained the following relationship between the mass flow rate of the fluid and the liquid film thickness:

$$\frac{\delta}{R} = \frac{3}{2}\left(\frac{\dot{m}\mu_L}{\pi\rho_L^2 g\delta^2 R^2} + \frac{\tau_i}{\rho_L g R}\right) \quad (12)$$

The shear stress at the liquid–vapor interface is a function of the relative velocity between the liquid and vapor flow:

$$\tau_i = \frac{\rho_v}{2}\left[\left(1 + \frac{\rho_v}{\rho_L}\frac{R}{2\delta}\right)\frac{\dot{m}}{\rho_v \pi R^2}\right]^2 \cdot C_{fi} \quad (13)$$

where the friction coefficient is correlated as a function of the Bond number and the liquid film thickness

$$C_{fi} = 0.005 + 0.2574\left(\frac{\delta}{R}\frac{Bo}{2}\right)^{1.63 + 4.74/Bo} \cdot 10^{9.07/Bo} \quad (14)$$

The flooding limit is the value of the heat transport rate for which Eq. (12) yields a unique value of δ.

Experimental Investigation

The working fluids used in the current experimental investigation were refrigerant-11, refrigerant-113, and ethanol. Experiments were conducted to measure the thermal resistance of the thermosyphon as a function of the heat transport rate over a range of saturation conditions corresponding to different condenser coolant temperatures.

Figure 1 illustrates the experimental apparatus used in the current study. The aluminum evaporator is heated by band heaters with a total maximum heat output of 820 W. The evaporator is covered with ceramic fiber insulation. The i.d. of the evaporator tube was machined to match that of the adiabatic and condenser sections (13.5 mm). The lengths of the thermosyphon sections are evaporator, 114 mm; adiabatic, 608 mm; and condenser, 330 mm. Thermocouples measure the temperature in the evaporator wall and the working fluid in

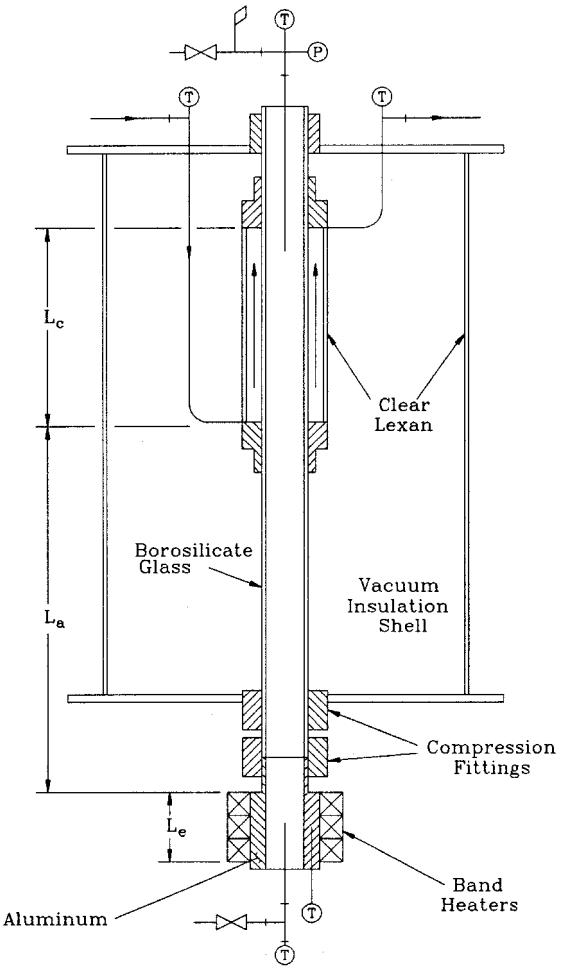

Fig. 1 Experimental apparatus.

the evaporator. The adiabatic and condenser sections were constructed of borosilicate glass tubing. The condenser is cooled by water flowing through the annulus formed by the clear polycarbonate condenser shell. The flow rate and inlet and outlet temperatures of the condenser coolant were measured to confirm the overall energy balance. The adiabatic and condenser sections are surrounded by a vacuum insulation shell constructed of a clear polycarbonate tube. A thermocouple probe in the condenser measured the working fluid temperature just below the condenser coolant outlet. A pressure transducer measured the pressure at the top of the condenser. The thermosyphon was designed to operate up to a temperature of 190°C and a pressure of 410 kPa.

The fill ratio (defined as the volume of liquid in the thermosyphon divided by the volume required to fill the evaporator) was 1.0 in all of the experiments. In a previous study of the effects of the amount of working fluid on the heat transport limit of thermosyphons, Shiraishi et al.[4] found that the optimum fill ratio is usually between 0.3–1.0. Most previous experimental investigations have been conducted with fill ratios less than 1.0.

The uncertainty in the heat transport rate was ±3.0% for the entire range of power settings. This uncertainty is shown as error bars in plots of the test results. Within the limits of uncertainty, the evaporator input power always agreed with the measured rate of heat transfer to the condenser coolant. The saturation temperature was based on the measured pressure. The uncertainty of the pressure measurements was ±7.6 kPa, corresponding to a maximum uncertainty of ±2.3 K in the saturation temperature. The condenser temperature agreed with the measured saturation conditions to within these limits, confirming the absence of noncondensible gases.

Results and Discussion

The flooding limit was determined by monitoring the thermal resistance of the thermosyphon, which was calculated by measuring the temperature difference between the evaporator tube and the condenser coolant (average of inlet and outlet) for a given heat transport rate. The thermal resistance decreased continuously with increasing heat transport rate until the flooding limit was reached, at which point the evaporator temperature increased rapidly.

At low heat transport rates, the thermosyphon exhibited countercurrent annular flow, with the liquid flowing in a stable laminar film. As the power increased, small waves appeared at the liquid–vapor interface. Eventually, a heat transport rate was reached at which the two-phase flow suddenly became unstable, resulting in churn flow. The vapor flowed upward in large vapor slugs. The liquid bridging the tube at the ends of these slugs moved in a turbulent pulsating manner. The transition to churn flow resulted in a sudden decrease in the evaporator temperature.

Eventually, the flooding limit was reached, at which point liquid would begin accumulating at the top of the condenser. The beginning of the liquid accumulation always coincided with an increase in thermal resistance. In test runs in which the power was increased past the flooding limit, the length of the liquid slug grew until it blocked a considerable portion of the condenser. Table 1 shows the flooding limits for the three working fluids used in the current experimental investigation along with the corresponding saturation temperatures.

Figures 2 and 3 compare data from the current experiments with the five predictive methods described earlier. In some cases, the scatter in data is greater than the uncertainty. This indicates that the predictive ability of the best flooding models will be limited to a relatively high uncertainty.

The correlation presented by Tien and Chung[2] yields good predictions for the refrigerant data, but tends to underpredict the ethanol data by approximately 20–30%. This is consistent with the observation that this correlation tends to predict low flooding limits for fluids with high liquid/vapor density ratios.[6]

Table 1 Flooding limits determined in current experimental study

Fluid	T_{sat}, °C	Q, W
Refrigerant-113	58.3	270.7
	71.0	291.9
	71.5	310.3
	80.9	311.0
Refrigerant-11	61.8	325.6
	66.3	311.0
	67.2	346.6
Ethanol	52.3	559.7
	60.1	600.0
	66.4	707.4
	94.1	816.7

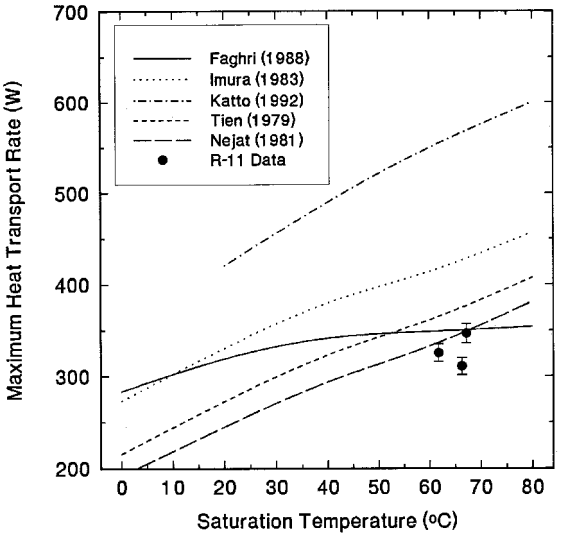

Fig. 2 Refrigerant-11 data from current experimental study.

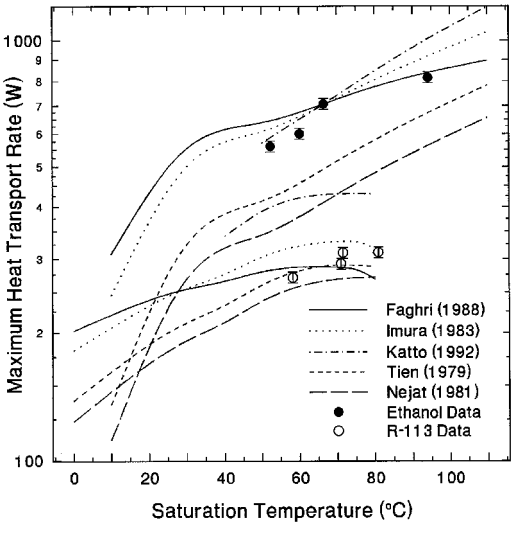

Fig. 3 Refrigerant-113 and ethanol data from current experimental study.

The correlation proposed by Nejat[5] yields similar results and suffers from the same drawback.

The flooding correlation by Faghri et al.[6] yields relatively good predictions for all of the data from the current study, predicting the flooding limit to within ±20% for all three fluids. It is evident from Table 2 that this correlation exhibits the lowest standard error of the five predictive methods considered here. The correlation by Imura et al.[7] overpredicts most of the